Supporting Information for

One Pot Synthesis of Magnetic Polypyrrole Aerogel with 1D/2D Hybrid Nanostructures for Microwave Absorption

Jianjian Yang[1]*; Lingyan Qin[1]; Guojie Liang[1]; Qizhi Zhao[1]; Kejun Wang[1]; Hua Yan[2]*; Zhide Hu[3]*

1 State key Laboratory of Nuclear, Biological and Chemical Protection for Civilian, Beijing 102205, China

2 Chongqing College of Architecture and Technology, Chongqing 401331, China

3 Army Logistics Academy, Chongqing 401331, China

*Corresponding Authors.

* Correspondence: yangjianjiancq@163.com (J Yang), 892496530@qq.com (H Yan), zhidehucq@163.com (Z Hu)

Supplementary Note 1. Experiment

Materials:

Pyrrole (Py), iron(III) chloride hexahydrate ($FeCl_3·6H_2O$), methyl orange (MO, sodium 4-[4-(dimethylamino)-phenylazo]benzenesulfonate), and epichlorohydrin (C_3H_5ClO) from Sinopharm Chemistry Reagent Co., Ltd. (China) were used as received. hydrochloric acid (HCl) and ethanol (99.5 %) were supplied by from Shanghai Macklin Biochemical Technology Co., Ltd., China. Deionized (DI) water was used in all experiments.

One pot synthesis of PPy-Fe aerogel:

Pyrrole monomer and MO with mole ratio of 1:0.02 was first added to the H_2O/ethanol (1:1) mixed solution to form a mixture. Next the $FeCl_3·6H_2O$ solution with H_2O/ethanol (1:1) as solvent was added dropwise to the Py solution with the mole ratio of n(Py):n(Fe^{3+})=1:1 under quickly stirring (about 250 r/min). The viscous PPy intermediate was via a process of oxidation polymerization of pyrrole with iron(III) chloride, in which branching and cross-linking of the linear assemblies occurred in the presence of structure directing agent. Then the epichlorohydrin and additional Fe^{3+} ion solution (with mole ratio of 10:1) was added dropwise in sequence with stirring to initiate the reactions of hydrolysis and polycondensation of iron salts. The homogeneous sol was then sealed and cooled in the ice bath for ~1 hours and aged in room temperature for another 24 h to form gels. The gels were then transferred to beakers in which 0.2 M hydrochloric acid was added to partly recover the polypyrrole base to polypyrrole salt and dissolved some of the iron oxides and exchanged several times with ethanol. Finally, the resulting PPy hybrid aerogel (denoted as PPy-Fex, x=1, 2, 3, represents the additional Fe^{3+} content) would be harvested via solvent-exchange and supercritical CO_2 drying process (45 °C and 10 MPa for 4 h). For comparison, pure fibrous PPy aerogel was synthesized via a conventional oxidation of pyrrole with iron(III) chloride in the presence of methyl orange.

Characterizations:

The morphology and microstructure of prepared samples were observed by scanning electron microscope (SEM, Thermo Fisher Scientific Apreo 2S+) and transmission electron microscope (Jem-2100F) equipped with an energy dispersive X-ray spectroscopy (EDS, X-MAX 65T). Thermogravimetric analysis (TGA, TGA550, USA) was performed in an air atmosphere at a test range of 40 °C to 600 °C with a ramp rate of 10℃/min to evaluate the magnetic phase content through:

$$\frac{2 \cdot R \cdot M(Fe_3O_4)}{3 \cdot M(Fe_2O_3)} + organic\% + water\% = 1 \qquad \text{(Eq. S1)}$$

where wt % R is the remaining weight percentage after combustion, and M indicates the molecular weight of the compound.

Specific surface areas were measured by nitrogen adsorption/desorption porosimetry using a BSD-PM surface area/pore distribution analyzer. Samples for surface area determination were outgassed at 150 °C for 2 h before analysis. The Brunauer-Emmett-Teller (BET) method was used to determine the total surface area (S_{BET}). The structural information and elemental analysis of the samples were determined by X-ray powder diffractometer (XRD, D8 Advance, Germany) utilizing Cu-Kα radiation with wavelength of 0.15406 nm in 2θ range of 10~90° and X-ray photoelectron spectroscopy (XPS, Thermo Fisher ESCALAB 250Xi) Al-Kα radiation (energy = 1486.8 eV) in vacuum. Magnetic hysteresis loop was measured by a vibrating sample magnetometer (VSM, 8604, Lake Shore, USA).

The electromagnetic parameters in the frequency range of 2-18 GHz were measured by a vector network analyzer (Agilent, E5071c, USA) using coaxial wire method according to the standard Nicolson-Ross-Weir (NRW) algorithm. The toroidal ring samples were prepared by mixing paraffin with as-prepared powders (grounded by a 200 meshes) and then pressed into a mold with outer diameter of 7.0 mm, inner diameter of 3.04 mm. As an electromagnetic wave absorption (EMWA) material, reflection loss (RL) and input impedence (Z_{in}) are the important evaluation indexes. According to transmission line theory, RL and Z_{in} can be calculated by the following formula [1-3]:

$$RL = 20\log\left|\frac{Z_{in} - Z_0}{Z_{in} + Z_0}\right| \quad \text{(Eq. S2)}$$

$$Z_{in} = Z_0\sqrt{\frac{\mu_r}{\varepsilon_r}}\tanh\left[\frac{j2\pi df}{c}\sqrt{\varepsilon_r\mu_r}\right] \quad \text{(Eq. S3)}$$

where, Z_0 is the intrinsic impedance of free space and Z_{in} is the input impedance of the absorber; c represents the velocity of light; The μ_r ($\mu_r = \mu^{'} - i\mu^{''}$) and ε_r ($\varepsilon_r = \varepsilon^{'} - i\varepsilon^{''}$) are complex permeability and permittivity of the absorber; *d* is the thickness of the absorbing materials; *f* is the frequency of microwaves.

The attenuation constant (α) can be calculated through

$$\alpha = \frac{\sqrt{2}\pi f}{c}\sqrt{(\mu^{''}\varepsilon^{''} - \mu^{'}\varepsilon^{'}) + \sqrt{(\mu^{'}\varepsilon^{''} + \mu^{''}\varepsilon^{'})^2 + (\mu^{''}\varepsilon^{''} - \mu^{'}\varepsilon^{'})^2}} \quad \text{(Eq. S4)}$$

The contribution of the magnetism to the microwave absorption performance comes mainly from natural resonance, eddy current loss and exchange resonance. The eddy current loss factor (C_0) can be expressed [4-6]:

$$C_0 = \mu^{''}(\mu^{'})^{-2}f^{-1} = 2\pi\mu_0 d^2\sigma \quad \text{(Eq. S5)}$$

where, σ is the electrical conductivity.

Supplementary Note 2. Electromagnetic simulation technology:

For evaluating the practical application of the three samples, further simulation was carried out based on far-field response using CST Studio Suite 2021. In this simulation, the tested model consists of the upper absorber layer and the bottom perfect electric conductor (PEC) layer, where the perfect electric conductor (PEC) and absorber are modeled as squares, which are specifically represented as an ultrathin PEC layer (200 × 200 mm) and an absorber layer (200 × 200 × 3.3 mm). The linearly polarized plane wave was defined as the excitation port, and the microwave propagates in the negative direction of the y-axis and the electric polarization direction is along the z-axis. The open (add space) boundary conditions were used in all directions. The scattering direction was determined by θ and φ. The radar cross section (RCS) of the simulated sample is expressed by the following equation.[13-14]

$$\sigma(dBm^2) = 10log\left[\frac{4\pi S}{\lambda^2}\left|\frac{E_s}{E_i}\right|^2\right] \quad \text{(Eq. S6)}$$

where, S is the area of the simulated plate, λ is the length of the incident microwave, E_s is the electric field intensity of transmitting waves, and E_i is the electric field intensity of receiving wave.

Supplementary Note 3. Figure and Table.

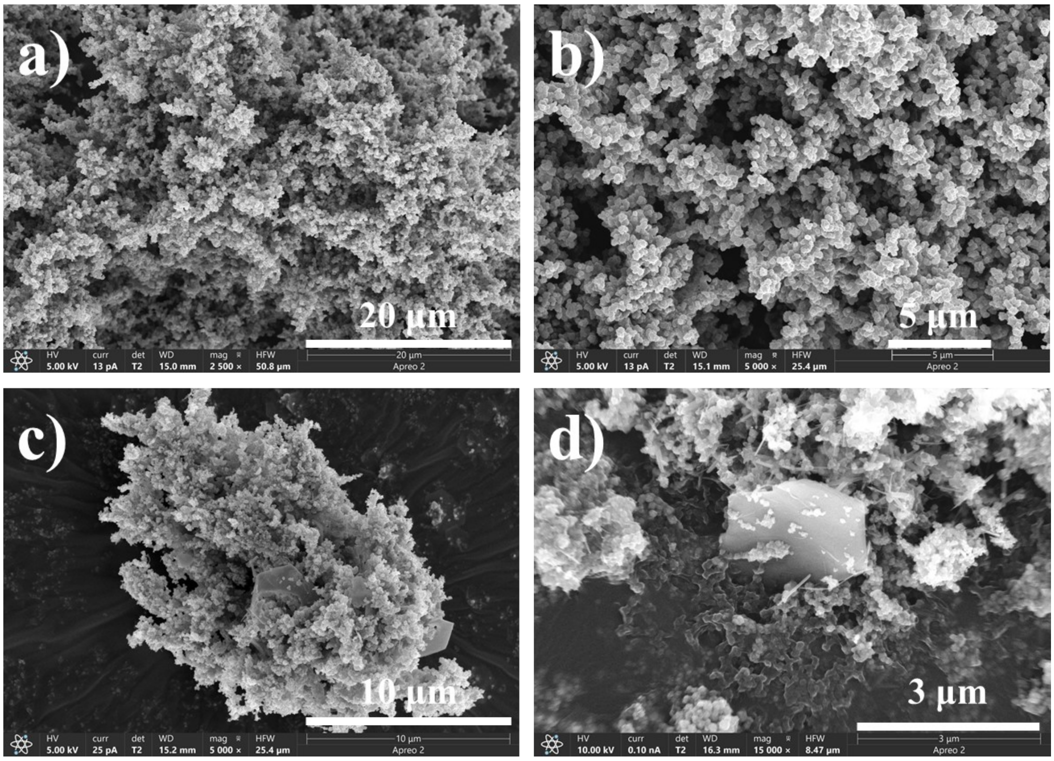

Figure S1. Scanning electron microscopy image of pure grabular PPy aerogel (a,b) and grabular PPy-Fe aerogel (c,d). The reference grabular PPy aerogels were prepared by the oxidation of pyrrole with iron(III) chloride in the absence of methyl orange.

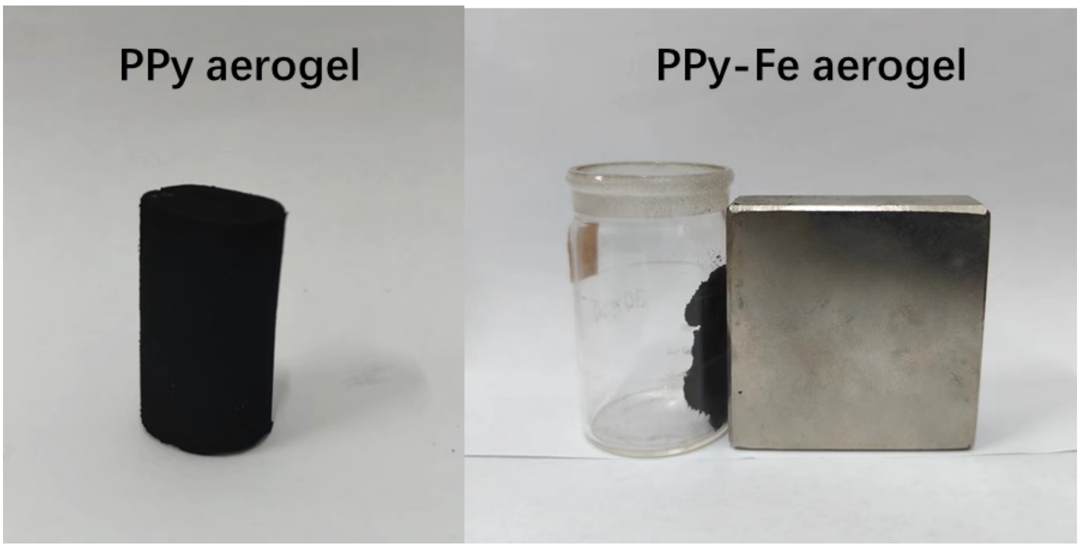

Figure S2. Photos of as-prepared pure PPy aerogel (left) and PPy-Fe2 aerogel. The PPy-Fe2 sample can be attracted to the external permanent magnet.

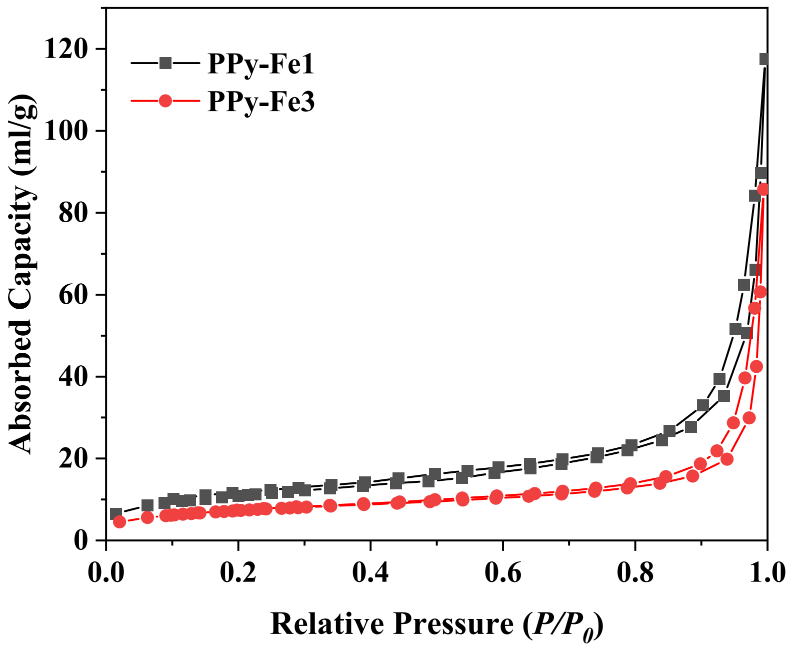

Figure S3. N_2 adsorption−desorption isotherms of PPy-Fe1 and PPy-Fe3 samples.

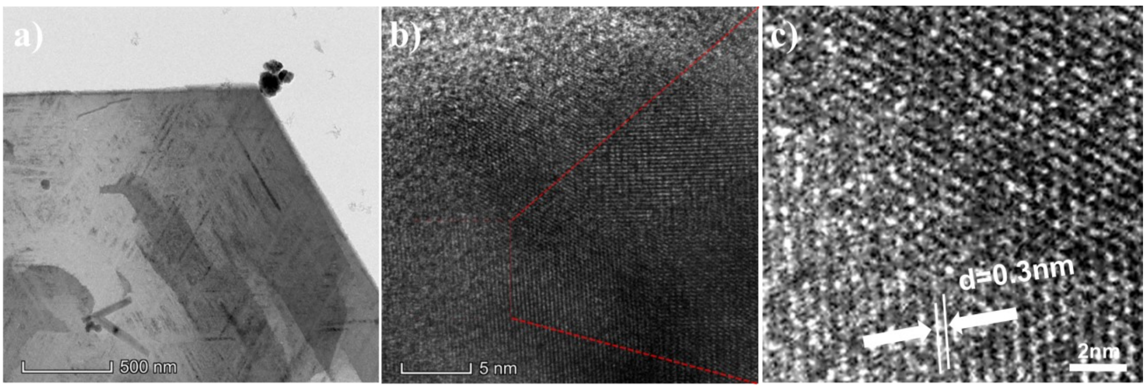

Figure S4. TEM image and HR-TEM image of PPy-Fe.

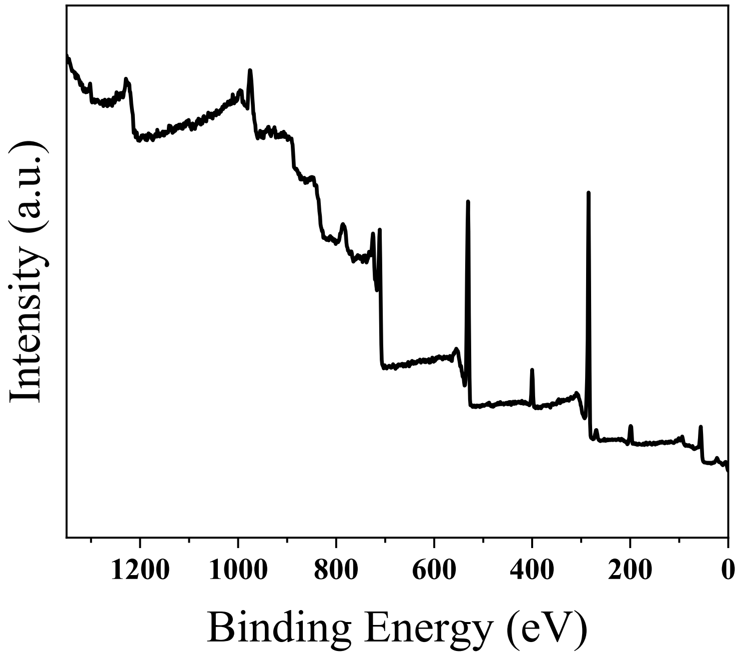

Figure S5. Survey XPS spectra of the PPy-Fe sample.

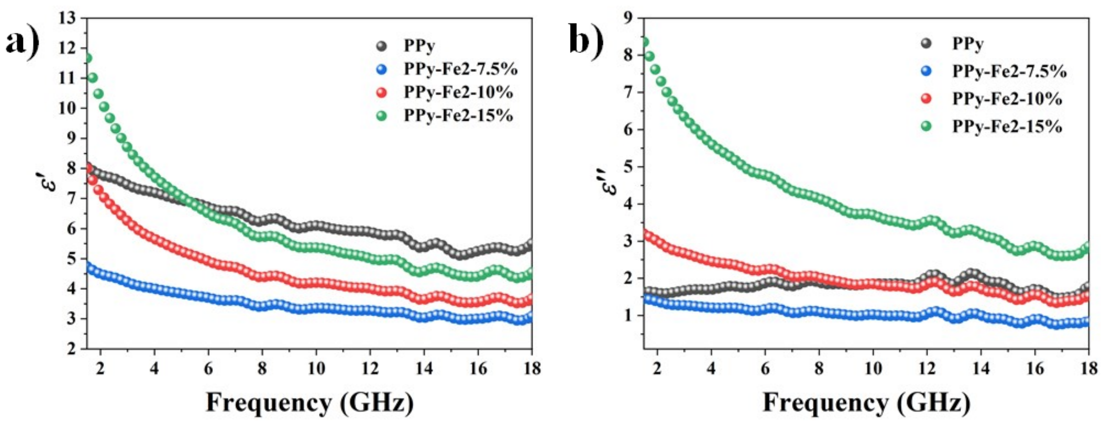

Figure S6. The plots of complex permittivity (a) ε' and (b) ε'' against filler ratios of PPy-Fe2 sample.

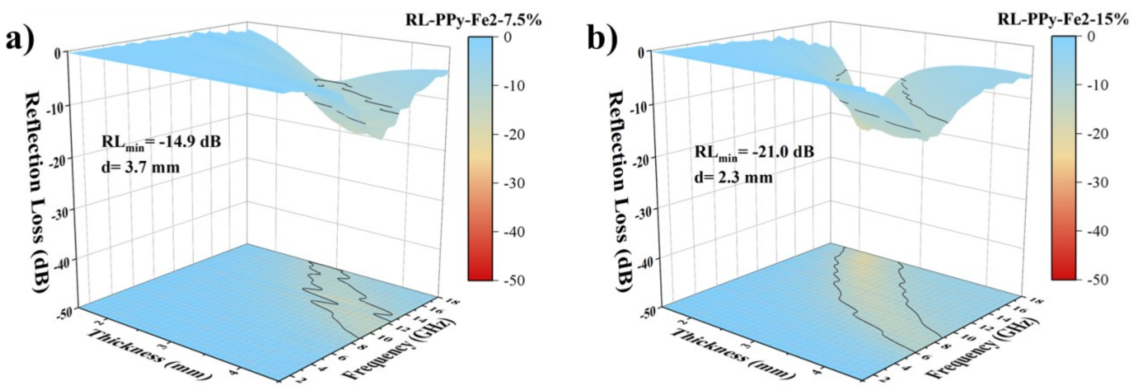

Figure S7. Three-dimensional representations and contour RL values versus frequency at different thicknesses samples for PPy-Fe2 with filler ratio of 7.5% and 15%, respectively.

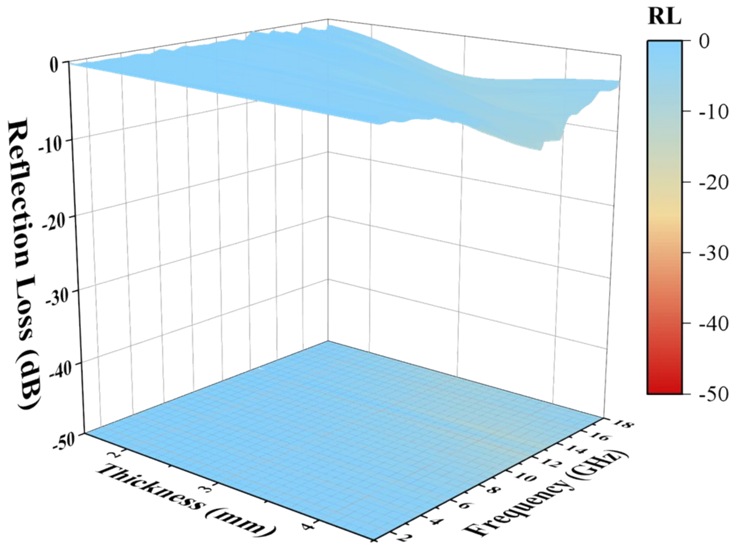

Figure S8. Three-dimensional representation and contour RL values versus frequency at different thicknesses samples for grabular PPy-Fe with filler ratio of 10%. Given the close similarities in component between the two samples, the higher performance of PPy-Fe2 compared to reference grabular PPy-Fe (at the same filler loading) was reasonably ascribed to the unique 1D/2D nanostructure of PPy-Fe2 aerogel.

Table S1 Comparison of microwave absorption performance between the PPy-Fe2 aerogel and recently reported absorbing materials.

Samples	Filler content (wt.%)	RL_{min} (dB)	EAB (GHz) RL < 10 dB	d (mm)	Ref.
Ni-SA/HPCF	10	-53.2	5	3.5	[7]
Ni/Co/CrN/CNTs-CF	10	-56.18	5.76	2.1	[8]
$HcFe_3O_4$@C	50	-46.4	5.0	3.5	[9]
Fe_3O_4/ZnO@C	50	-40.0	6.0	2.0	[10]
Fe_3C/Fe_3N@C	10	-58.6	6.6	2.62	[11]
CC@$NiCo_2O_4$	-	-54.1	6.3	2.0	[12]
rGO/MOF foams	15	-60.13	6.23	4.84	[13]
Ni@NPC	5	-72.4	5.0	3.0	[14]
G/C/Fe_3O_4	20	-37.2	4.16	3.0	[15]
CNT@NiCo	10	-50.1	6.1	2.0	[16]
PPy-Fe2	10	-42.6	7.13	3.3	This work

Supplementary references

[1] Liang, Jie et al. Defect-engineered graphene/Si_3N_4 multilayer alternating core-shell nanowire membrane: a plainified hybrid for broadband electromagnetic wave absorption. Advanced Functional Materials, 2022, 32(22): 2200141.

[2] Tian, Yingrui et al. Graphene-based aerogel microspheres with annual ring-like structures for broadband electromagnetic attenuation. Chemical Engineering Journal, 2023, 464: 142644.

[3] Qu, Ning et al. 2D/2D coupled MOF/Fe composite metamaterials enable robust ultra-broadband microwave absorption. Nature Communication, 2024, 15(1): 5642.

[4] Yang, Bintong et al. One-dimensional magnetic FeCoNi alloy toward low-frequency electromagnetic wave absorption. Nano-micro Letters, 2022, 14(1):170.

[5] Guo, Yuan et al. Boosting conductive loss and magnetic coupling based on "Size Modulation Engineering" toward lower-frequency microwave absorption. Small, 2023, e2308809.
[6] Li, Shuangshuang et al. Graphene-based magnetic composite foam with hierarchically porous structure for efficient microwave absorption. Carbon, 2023, 207: 105-115.
[7] Zhang, X. et al. Metal ions confined in periodic pores of MOFs to embed single-metal atoms within hierarchically porous carbon nanoflowers for high-performance electromagnetic wave absorption. Advanced Functional Materials, 2023, 33, 2210456.
[8] Zhu, J et al. Porous structure fibers based on multi-element heterogeneous components for optimized electromagnetic wave absorption and self-anticorrosion performance. Small, 2024, 240368.
[9] Deng, Y. et al. A novel and facile-to-synthesize three-dimensional honeycomb-like nano-Fe_3O_4@C composite: Electromagnetic wave absorption with wide bandwidth. Carbon, 2020, 169:118-128.
[10] Meng, X. et al. Three-dimensional (Fe_3O_4/ZnO)@C double-core@shell porous nanocomposites with enhanced broadband microwave absorption. Carbon, 2020, 162: 356.
[11] Hu, R. et al. Enhanced electromagnetic energy conversion in an entropy-driven dual-magnetic system for superior electromagnetic wave absorption. Advanced Functional Materials, 2024, 2418304
[12] Li, Xiao et al. Magnetic array vertically anchored on flexible carbon cloth with “magical angle” for the increased effective absorption bandwidth and improved reflection loss simultaneously. Carbon, 2023, 210(15): 118046.
[13] Li, S. et al. Graphene-based magnetic composite foam with hierarchically porous structure for efficient microwave absorption. Carbon, 2023, 207:105-115.
[14] Yang, W. et al. Magnetic coupling engineered porous dielectric carbon within ultralow filler loading toward tunable and high-performance microwave absorption. Journal of Materials Science & Technology, 2021, 70: 214-223.
[15] Pang, X. et al. Optimization of electromagnetic absorption properties based on graphene, carbon nanotubes, and Fe_3O_4 multidimensional composites. Polymer Compsites, 2024, 45(9):8414-8425.
[16] Zhao, Y. et al. Simultaneous optimization of conduction and polarization losses in CNT@NiCo compounds for superior electromagnetic wave absorption. Journal of Materials Science & Technology, 2023, 166: 34-46.